Phys. Status Solidi A **209,** No. 9, 1675–1682 (2012) / **DOI** 10.1002/pssa.201200581

physica status solidi a
www.pss-a.com
applications and materials science

Part of Topical Section on
Fundamentals and Applications of Diamond

Grain size tuning of nanocrystalline chemical vapor deposited diamond by continuous electrical bias growth: Experimental and theoretical study

Vincent Mortet[1,2,3], Liang Zhang[4], Maxie Eckert[5], Jan D'Haen[1,2], Ali Soltani[6], Myriam Moreau[7], David Troadec[6], Erik Neyts[5], Jean-Claude De Jaeger[6], Jo Verbeeck[4], Annemie Bogaerts[5], Gustaaf Van Tendeloo[4], Ken Haenen[*,1,2], and Patrick Wagner[1,2]

[1] Institute for Materials Research (IMO), Hasselt University, Wetenschapspark 1, 3590 Diepenbeek, Belgium
[2] IMOMEC, IMEC vzw, Wetenschapspark 1, 3590 Diepenbeek, Belgium
[3] LAAS, CNRS, Université de Toulouse, 7 Avenue du Colonel Roche, 31077 Toulouse, France
[4] Electron Microscopy for Materials Science (EMAT), University of Antwerp, Groenenborgerlaan 171, 2020 Antwerpen, Belgium
[5] Research Group PLASMANT, Department of Chemistry, University of Antwerp, Campus Drie Eiken, Universiteitsplein 1, 2610 Antwerpen, Belgium
[6] Institut d'Electronique de Microélectronique et de Nanotechnologie, CNRS UMR 8520, Cite Scientifique, Avenue Poincaré, 59652 Villeneuve d'Ascq Cedex, France
[7] Laboratoire de Spectrochimie Infrarouge et Raman, Université des Sciences et Technologies de Lille, Bâtiment C5, 59655 Villeneuve d'Ascq Cedex, France

Received 16 August 2012, accepted 22 August 2012
Published online 7 September 2012

Keywords bias, chemical vapor deposition, molecular dynamics, nanodiamond, Raman spectroscopy, transmission electron microscopy

* Corresponding author: e-mail ken.haenen@uhasselt.be, Phone: +32 11 26 88 75, Fax: +32 11 26 88 99

In this work, a detailed structural and spectroscopic study of nanocrystalline diamond (NCD) thin films grown by a continuous bias assisted CVD growth technique is reported. This technique allows the tuning of grain size and phase purity in the deposited material. The crystalline properties of the films are characterized by SEM, TEM, EELS, and Raman spectroscopy. A clear improvement of the crystalline structure of the nanograined diamond film is observed for low negative bias voltages, while high bias voltages lead to thin films consisting of diamond grains of only ~10 nm nanometer in size, showing remarkable similarities with so-called ultrananocrystalline diamond. These layers arecharacterized by an increasing amount of sp^2-bonded carbon content of the matrix in which the diamond grains are embedded. Classical molecular dynamics simulations support the observed experimental data, giving insight in the underlying mechanism for the observed increase in deposition rate with bias voltage. Furthermore, a high atomic concentration of hydrogen has been determined in these films. Finally, Raman scattering analyses confirm that the Raman line observed at ~1150 cm^{-1} cannot be attributed to trans-poly-acetylene, which continues to be reported in literature, reassigning it to a deformation mode of CH_x bonds in NCD.

1 Introduction The tremendous current interest in nanocrystalline diamond (NCD) particles and thin films is attributed to the vast range of possible applications for this material. Ample examples can be found in fields as microbiology (as fluorescence emitter, for cell therapy…), quantum computing, N/MEMS, chemical vapor deposition growth, biosensors, etc. [1–10]. The most used technique to produce NCD particles is based on a detonation process, which is unfortunately a cumbersome and hard to control industrial process [1].Therefore, other and easier to control means are currently receiving a lot of interest. The top-down approach, where NCD particles are produced starting from CVD diamond films with a well-controlled purity and grain size, seems to be particularly suitable [11]. In addition, recent

investigations have shown it is possible to incorporate 1–3 at% of boron atoms in NCD films with grain sizes ranging from 100 to 350 nm in diameter [12]. Even though such NCD grains are surrounded by a thin amorphous shell, the boron atoms are isolated, substitutional atoms embedded tetrahedrally into the diamond lattice, with no preferential embedding in the grain boundaries [13]. These findings open opportunities to produce (heavily) B-doped nanoparticles. To reach this goal, a thorough control is needed over grain size and phase purity. Although the use of substrate bias during the early stage of growth has been proven to be an efficient method for diamond nucleation, it is also an efficient mean to reduce the diamond grain size in films [14–16]. In this work, we report on structural and theoretical studies of NCD thin films grown by a continuous bias assisted CVD growth technique. As will be shown, this technique allows tuning of the grain size and phase purity of the deposited material.

2 Experimental

2.1 Nanocrystalline diamond films The thin diamond films were grown on 500 μm thick silicon substrates (one centimeter in diameter) by microwave plasma enhanced chemical vapor deposition (MW PE CVD) in a hybrid home-built NIRIM-type reactor [17] with different DC substrate bias voltages (V_b) applied during the complete duration of nucleation and growth. Prior to the diamond film deposition, the substrates were first heated to 700 °C in pure hydrogen plasma at 50 mbar. Subsequently, the samples were bias enhanced nucleated in a 1% methane in hydrogen mixture at a pressure of 50 mbar, a power of 275 W and a bias voltage of $-V_b = 260$ V. Finally, films were grown in the same 1% methane in hydrogen mixture at a pressure of 80 mbar and a power of 425 W during 1 h with DC bias voltage. Several diamond layers were grown using different bias voltages.

2.2 Characterization Several techniques were used: Raman scattering spectroscopy, scanning electron microscopy (SEM), transmission electron microscopy (TEM) and electron energy loss spectroscopy (EELS). Raman scattering measurements were carried out at room temperature using four different excitation wavelengths with a micro-spectrometer Labrum HR UV (Horiba Scientific). SEM images were obtained in secondary electron mode with a FEI Quanta 200 FEG–SEM. Samples for TEM investigations were prepared by focused ion beam in two steps. First, the samples were milled with a Ga+ beam at an acceleration voltage of 30 kV and a beam current of 1 nA. Finally, both sides of the foil were milled at an acceleration voltage 5 kV and 1 nA beam current to remove the amorphous layer that might be formed in the first step. TEM analyses were carried out in a Philips CM 20 microscope and a CM 30 microscope. The latter is equipped with a Schottky field emission gun (FEG) and a Gatan imaging filter system (GIF 200) for EELS with an energy resolution of 0.9 eV.

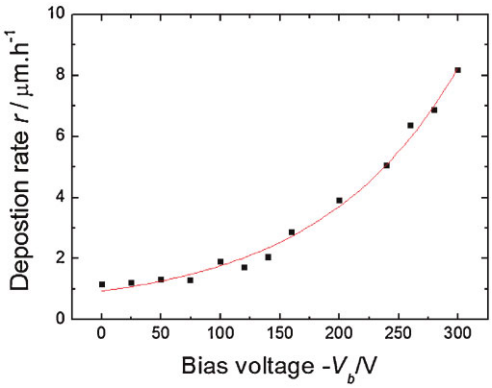

Figure 1 (online color at: www.pss-a.com) Deposition rate as a function of the bias voltage ($-V_b$). The curve through the data points is an exponential fit.

3 Experimental results and discussion In Fig. 1, the variation of the deposition rate of the films as a function of the bias voltage is shown. Thicknesses were measured by SEM on cross sections of the deposited films. As can be seen, the deposition rate slowly rises for low bias voltages, followed by an exponential increase for $-V_b > 100$ V. Note that for clarity, when bias voltage is mentioned in the remainder of the text, it always refers to the absolute value of the negative bias voltage, i.e. $-V_b$. This behavior, previously observed by others, is usually mainly related to the increase of the substrate current, i.e. the flux of hydrocarbon ionized species arriving at the substrate surface, but also to the related temperature rise of the substrate due to the increasing bias voltage and the consequent particle flux [18–20]. The nearly exponential increase of the substrate current can thus be directly related to the observed increase of deposition rate. The molecular dynamics (MD) simulations described in Section 3 will shed more light on the fundamental processed responsible for these observations.

To further investigate the effect of the increasing ion flux, Fig. 2 shows the surface morphology observed by SEM of the as-deposited films as a function of $-V_b$. Polycrystalline diamond films consisting of facetted grains are clearly identified on these images for bias voltages between $-V_b = 0$ and 200 V. Between $-V_b = 0$ and 75 V the films exhibit a (110) preferential growth orientation, with characteristic pyramidal shaped grains [21]. Moreover, the average grain size slightly increases as the absolute bias voltage increases. At bias voltages of $-V_b = 100$ and $-V_b = 120$ V, the observed preference has shifted towards a (100) orientation with the typical squared facetted grains [22]. Once the bias voltage is larger than $-V_b = 140$ V, the average grain size decreases and all preferential orientation is lost. At $-V_b > 200$ V, the surface morphology changes even more significantly becoming smooth with a root mean square roughness that is reduced from ~50 nm at $-V_b = 140$ to ~10 nm, as measured on a 4×4 μm^2 squared surface. These films seem to be made of much finer grains with a diameter below 30 nm, resembling much more to the so-called

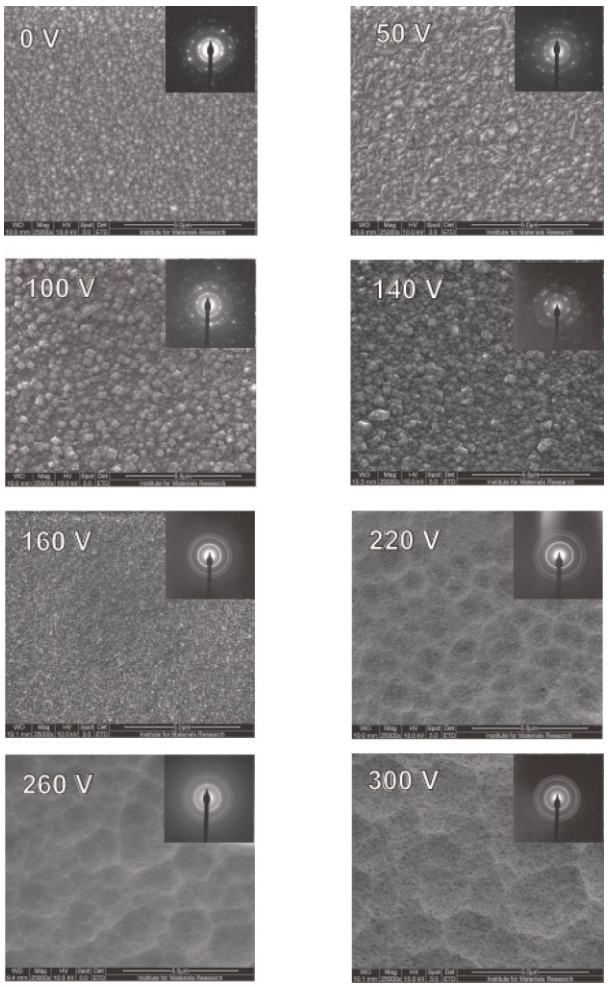

Figure 2 SEM images of the film surfaces grown at different bias voltages. TEM diffraction patterns are shown as insets and are taken from cross sections of the same samples.

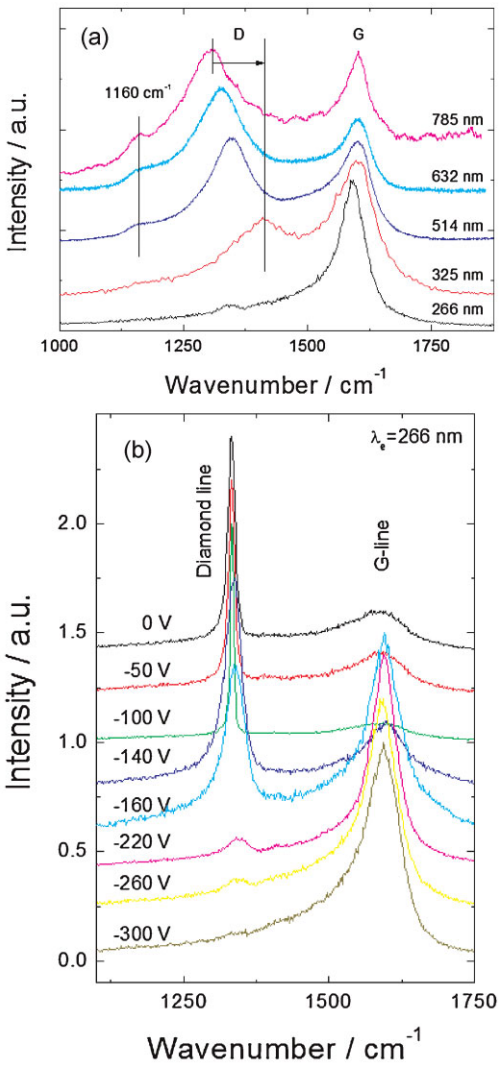

Figure 3 (online color at: www.pss-a.com) (a) Raman scattering spectra for a film deposited at a bias voltage $-V_b = 260$ V obtained using different excitation wavelengths: 266 nm, 325 nm, 514 nm, 632 nm and 785 nm. (b) Raman scattering spectra of the diamond films as a function of the bias voltage (V_b), taken with 266 nm illumination. The curves are shifted vertically for clarity.

ultrananocrystalline diamond (UNCD) films, usually grown using hydrogen-poor plasmas, in contrary to nanocrystalline (NCD) films that are grown in gas mixture similar to that used in this work [23].

To assess the composition of the different layers, all samples were characterized by Raman spectroscopy using different excitation wavelengths, from infrared (775 nm) to ultra-violet (266 nm). All samples exhibit a strong photoluminescence and a large disordered graphitic (D) line contribution that shifts, from ~ 1300 to $\sim 1400\,\mathrm{cm}^{-1}$, in IR and visible Raman but not in UV Raman scattering measurements [24]. Raman scattering spectra obtained on a sample grown with a bias voltage $-V_b = 260$ V are shown in Fig. 3a. These spectra also exhibit the graphite (G) line ($\sim 1600\,\mathrm{cm}^{-1}$), and a shoulder at $\sim 1150\,\mathrm{cm}^{-1}$. Surprisingly, up to date, new literature is appearing where the latter is still assigned to trans-poly-acetylene despite that this substance is known to decompose at temperatures far below the deposition temperatures used in most of the CVD diamond experiments, i.e. 700–900 °C [25–27]. While the D line shifts to higher wave numbers and decreases in intensity relatively to the G line as the photon energy (E_{ph}) of the excitation laser increases, it disappears when UV excitation is used [24]. Besides the G band, the UV Raman spectrum shows a minute and relatively broad band at $1341\,\mathrm{cm}^{-1}$ that is ascribed to Raman scattering of nanometer sized diamond grains. UV Raman scattering spectra of the different thin films are shown in Fig. 3b. Only the diamond line at $\sim 1333\,\mathrm{cm}^{-1}$ and the G-line at $\sim 1600\,\mathrm{cm}^{-1}$ are clearly observed on these spectra for all bias voltages below $-V_b = 200$ V. The former line is also the most intense line for bias voltages between $-V_b = 0$ and $-V_b = 140$ V, while the sharpest diamond line is observed at a bias voltage $-V_b = 100$ V. For absolute values of the bias voltage higher

than 200 V, this line is significantly broadened and decreased in intensity compared to the G peak. The broadening of the diamond line is a signature of disorder in the diamond phase or a decrease in the grain size while the increase of the G-line intensity has to be linked to an increase in the volume fraction of graphite to diamond in the films. The tiny line observed at $\sim 1340\,\mathrm{cm}^{-1}$, on spectra of films grown at high bias voltage ($-V_b \geq 220$V), is assigned to NCD under compressive stress ($\sigma \sim 6$–7 GPa) [28], with a grain size estimated to be 7–8 nm [29, 30]. This large stress is consistent with the observed low radius of curvature (2 cm) of the silicon substrate after the thin film deposition. These films were also characterized by IR transmission measurements on which a significant absorption band between 2800 and $3000\,\mathrm{cm}^{-1}$ of sp^3 CH_x bonds' stretching vibration modes is observed (not shown). The atomic concentration of hydrogen in the film has been estimated to exceed $3 \times 10^{22}\,\mathrm{cm}^{-3}$ from the CH_x absorption band using the Beer–Lambert law and a thin polyethylene reference film used to determine the absorption coefficient of CH bonds. On the other hand, none of the well-known absorption bands of trans-poly-acetylene (at $\sim 1000\,\mathrm{cm}^{-1}$, $1800\,\mathrm{cm}^{-1}$, and $\sim 3045\,\mathrm{cm}^{-1}$) are observed. In addition, the Raman band at $1160\,\mathrm{cm}^{-1}$ does not significantly shift with the excitation energy (see Fig. 3a) as expected for trans-poly-acetylene [31]. Hence, these results clearly disagree with previous reports suggesting that the Raman scattering band at $\sim 1150\,\mathrm{cm}^{-1}$ is due to trans-poly-acetylene. We therefore argue that this line has to be reassigned to a deformation mode of CH_x bonds, a conclusion that seems to be supported by recent deuteration experiments [32].

TEM diffraction patterns of the diamond film cross-sections are shown as insets in Fig. 2 together with the SEM images as a function of bias voltage. These diffraction patterns clearly show the variation of the crystallinity of the films. At low bias voltages ($-V_b < 140$ V), the samples are crystalline, with large grain sizes as evidenced by the spots in the diffraction patterns and the well-known columnar structure, which is obvious in SEM [33]. For higher bias voltages, the films consist of very small grains, a fact that is supported both by the SEM images and the smearing of the diffraction spots into typical diffraction rings which can be identified as belonging to the diamond phase. An average grain size of ~ 10 nm has been determined using dark field images of the (111) diffraction ring for films grown at a bias voltage $-V_b = 280$ V. The crystallinity, i.e. the ratio between crystalline diamond and amorphous carbon has been determined using the shape of the carbon K-edge in the EELS spectra. The carbon K-edge (excitations from the 1s core state to an unoccupied state) is very sensitive to the local environment as can be seen by the dramatic changes in fine structure for the reference materials amorphous carbon and diamond in Fig. 4a. A linear combination fit of both reference spectra is used to determine the ratio between amorphous carbon and diamond taking into account the effect of multiple scattering and background [34, 35]. The result of such a fit is shown in Fig. 4b and clearly shows an increase in crystalline diamond content of up to 92% between

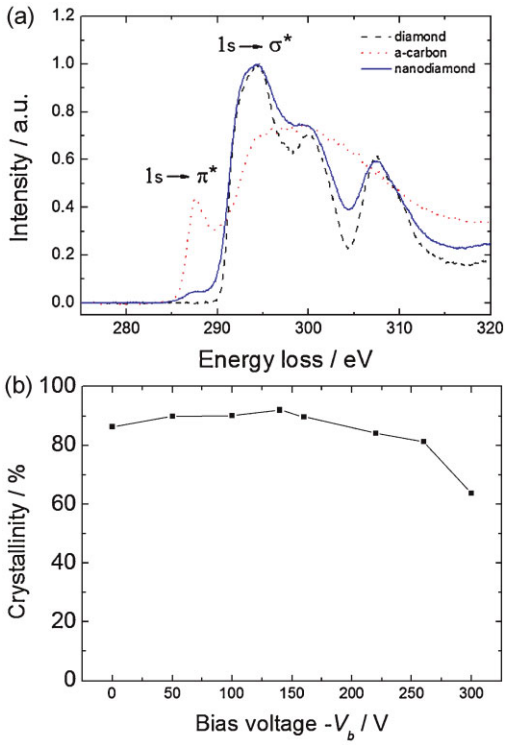

Figure 4 (online color at: www.pss-a.com) (a) EELS spectrum of a carbon K-edge for a film grown at $-V_b = 280$ V and the diamond and amorphous carbon reference spectra. The sharp peak at the absorption edge corresponds to the excitation of the carbon K-shell electron (1s electron) to the empty anti-bonding pi-band (π^*) while the most intense peak corresponds to the exitation of the carbon K-shell electron to the empty anti-bonding pi-band (σ^*). (b) Crystalline diamond content as a function of bias voltage obtained from a linear combination fit of the carbon K-edges from pure diamond and amorphous carbon to the carbon K-edge, and this for the different growth conditions.

$-V_b \sim 140$–160 V after which it significantly decreases down to 64% with a further increase in bias voltage. These results are consistent with the Raman scattering results, that show that the crystallinity of the films increases with bias voltage ($-V_b$) up to ~ 100–140 V and that higher bias voltages induce a significant increase of the non-diamond phase. As the average grain size remains around ~ 10 nm, i.e. sp^3-bonded diamond, this increase must be situated in the surrounding sp^2-bonded carbon matrix in which the diamond grains are embedded.

In summary, after a small improvement of the crystallinity at low bias voltages $-V_b \leq 150$ V, there is a significant diamond grain size reduction and the films consist of NCD grains. Among the large variety of NCD films, these films are different from diamond grown from conventional reactive hydrogen–methane mixtures, but similar to UNCD films usually grown in argon rich, i.e. hydrogen deficient plasmas, and to films grown under a prolonged energetic plasma bombardment by DC glow discharge. The first process relies on a very high nucleation density and such films can only be

grown as a thin layer due to the obvious grain enlargement with the film thickness [36]. On the other hand, during UNCD growth, there is a continuous diamond grain renucleation that limits the grain size. Such films consist of diamond grains with a size of 3–5 nm with abrupt grain boundaries [36, 37]. They can be grown thick and smooth, retaining these small grain sizes, contrary to NCD growth. A similar grain size can be obtained by DC glow discharge. As described by Hoffman et al. [38] film growth with this technique occurs from energetic species being accelerated and incorporated into the film surface. This process, known as subplantation [39], is based on the formation of a dense, hydrogenated sp^2-bonded layer, which in turn, partly evolves into sp^3-bonded diamond particles due to preferential displacement of the sp^2-bonded carbon atoms under bombardment by energetic species, sufficiently present in a DC glow discharge. It is clear that a continuous bias voltage can lead to a similar process, explaining the specific morphology observed at higher bias voltages, i.e. a large concentration non-diamond carbon phase, and a large concentration of atomic hydrogen. However, the layers grown with continuous electrical bias have a slightly larger grain size than the DC glow discharge films.

4 Molecular dynamics simulations Classical MD simulations have been carried out in order to have a deeper understanding of the experimental results. A sample computationally mimicking NCD growth, i.e. diamond shelled by an amorphous phase, was bombarded by hydrocarbon species with kinetic energies according to bias voltages between 10 and 200 V, i.e., kinetic energies between 5 and 80 eV. As experimentally measured by Kátai et al. [18], most ion energy distributions show a peak at 15–40% of the bias voltage.

In MD, the atoms of the considered system interact through a potential function, based on Newtonian dynamics [40]. By integrating the equations of motion, the positions and velocities of the atoms are calculated for each discrete time step during the simulation. The MD model is based on a code that was originally developed by Tanaka et al. [41]. The interactions of the atoms are modeled by the Brenner potential for hydrocarbons [42]. The Brenner potential is an empirical potential function. The binding energy of the system that is considered in the simulation is written as a sum over bond energies between couples of atoms. The bond energy is determined by repulsive and attractive components, which are functions of the scalar separation between the two considered atoms.

The simulated sample composed of a crystalline and an amorphous phase was prepared from a perfect diamond (100)2 × 1:2 H substrate consisting of 1920 C and 48 H atoms. The lower 100 atoms (two atomic layers) are kept fixed to anchor the simulation cell, preventing its translation due to momentum transfer from impacting particles. In order to obtain a sample that mimics the experimentally observed structure, atomic hydrogen was incorporated into the diamond substrate. For the incorporation of atomic hydrogen into CVD diamond [43], the diamond (100)2 × 1:2H surface was impacted by 60 H atoms. Due to collisions in the plasma sheath region, their kinetic energies are distributed according to the Maxwell distribution with $E_{rms} = 60$ eV, which corresponds to a substrate bias of 150 V [18] A substrate temperature of 1350 K was achieved by applying the Berendsen heat bath algorithm [44].

In Fig. 5a, the resulting sample, i.e. the input configuration for the theoretical investigation, is shown. It has dimensions of 14.0 Å × 21.0 Å × 41.8 Å, and contains now 82 hydrogen atoms. The 48 hydrogen atoms originating from the former perfectly hydrogenated diamond surface are still located very close to or at the surface. Besides those H atoms, the simulated sample contains 34 H atoms resulting from the H impacts, as described above. This hydrogen concentration of 2.8×10^{21} cm^{-3} approaches well the experimentally measured concentration of 3×10^{21} cm^{-3} (see above). Regarding the location of the implanted H atoms, the obtained structure fits the theoretical predictions by Michaelson et al. [43]: although hydrogen atoms are present in the diamond phase, most of the hydrogen is located in the amorphous phase. At the sharp interface between the amorphous and crystalline phase, the hydrogen concentration is rather low, and the hydrogen remains at the amorphous side of the interface.

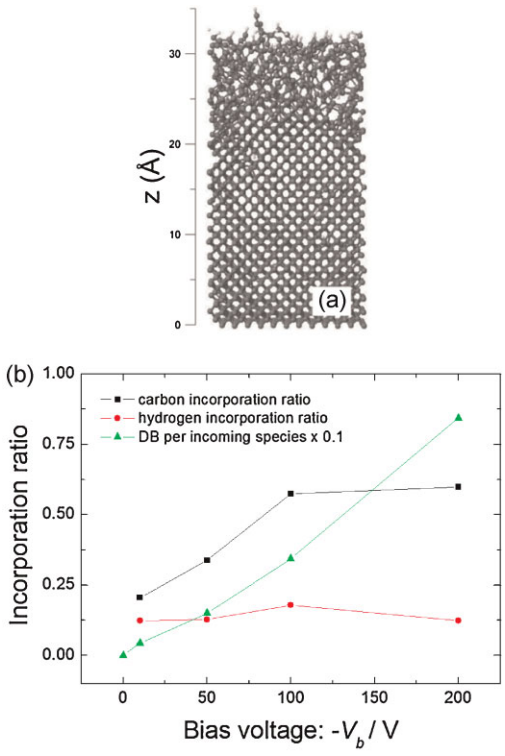

Figure 5 (online color at: www.pss-a.com) (a) The input cell with 1920 C atoms (dark gray) and 82 H atoms (light gray) for diamond growth MD simulation at different bias voltages. The {*x*,*y*} plane lies perpendicular to the *z*-axis. (b) Calculated carbon and hydrogen incorporation ratio and the formation rate of dangling bonds after 160 simulated impacts of hydrocarbon species as a function of the bias voltage ($-V_b$).

This structure, shown in Fig. 5a, is cumulatively bombarded by hydrocarbon species. The relative fluxes of the hydrocarbon species and kinetic energies were taken from Ref. [18]. Kátai et al. measured the ion fluxes and the ion energy distributions of the most important bombarding species as a function of the bias voltage (varying from 0 to 200 V), applying similar growth conditions of diamond as in our study, i.e. a microwave plasma of CH_4 with a surplus of H_2.

At low bias (<50 V), the main hydrocarbon species are H_3^+, CH_3^+, CH_4^+, and $C_2H_3^+$, whereas at high bias voltages (> 100 V), H^+, C^+, CH^+, CH_2^+, C_2H^+, $C_2H_2^+$, $C_2H_3^+$ are dominant [18]. In our model, ions are represented by neutral hydrocarbon species, assuming that all the ions are Auger-neutralized before reaching the surface, that is, the ions are neutralized by an emitted electron from the surface [45].

All simulated impacts are normal to the surface and calculated one by one during a time of 5.0 ps using variable time steps between 10^{-7} and 10^{-4} ps. The initial z-coordinate above the surface is chosen such that the interaction energy between the surface atoms and the impacting species is negligible, and the position in the $\{x,y\}$ plane is chosen randomly. The kinetic energy of the impacting species is distributed according to the Maxwell distribution function with E_{rms} values reported by Kátai et al. [18], varying for the different hydrocarbon species and bias voltages. The rotational and vibrational energies correspond to a typical gas temperature of 2120 K above the substrate surface [46]. The substrate was cooled back to 1350 K after 3.0 ps of each trajectory, applying the Berendsen heat bath [44].

All simulations consist of 160 consecutive impacts. Since we simulate the impacts one by one and each during the same integration time (5.0 ps), the effect of the substrate bias on the absolute flux of species is not simulated: the experimentally observed enhanced flux when raising the bias voltage is not reflected by our simulation conditions. However, the relative fluxes of the impacting species and of course the ion energies are selected according to the experimental bias voltage, and these effects are probably more important.

Figure 5b shows the increase of dangling bonds per incoming species and the increase of carbon and hydrogen atoms in the sample normalized to their respective incoming flux, i.e. the incorporation ratios, as a function of the bias voltage. As shown in this figure, the incorporation ratio of carbon atoms increases with the absolute value of the bias voltage. It significantly increases at low bias voltage ($-V_b < 100$ V). The increase of the incorporation ratio is less pronounced for bias voltage between −100 and −200 V. The number of dangling bonds created during the bias is steadily increasing. This implies that the carbon species have a higher probability to form bonds with the diamond substrate at large bias voltages. This is certainly due to the increase of unbound electrons. Therefore, we can conclude that the almost exponential increase of the deposition rate with the bias voltage (see Fig. 1) is not only due to the increased flux of species to the growing film, as pointed out by Kátai et al. [18] but it is also due to the increase of carbon atom incorporation ratio, certainly linked to the increase of dangling bonds. Surprisingly, the incorporation ratio of hydrogen atoms is rather constant, it appears to have a weak maximum at $-V_b = 100$ V.

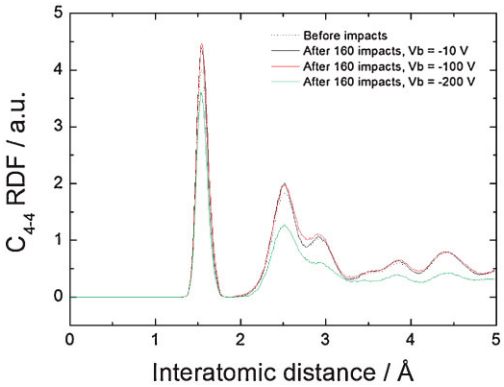

Figure 6 (online color at: www.pss-a.com) Normalized C4–4 radial distribution function of the original structure (dotted line), and after 160 impacts of the dominant bombarding species (see text) at substrate biases of respectively 10, 100, and 200 V (full lines). In order to measure the change of crystallinity in the amorphous phase and at the interface of crystalline and amorphous phases, only the upper parts of the simulated samples are taken into account, i.e. the atoms with z coordinates greater than 18.0 Å.

Figure 6 shows the four-coordinated carbon atoms radial distribution function (RDF), i.e. the variation of atomic density as a function of the distance, in the diamond cell after the MD simulations made at different bias voltages. Crystalline materials exhibit a RDF with well-defined peaks and valleys over a long length scale that characterizes the long-range order of these materials. On the other hand, RDF exhibit less pronounced or no peaks in amorphous materials, especially for the longer length scale.

The first neighbor interaction peak of samples obtained with bias voltages $-V_b = 10$ V and $-V_b = 100$ V has a higher intensity than the original sample. Furthermore, the maxima on long-range scale also rise, indicating that the long-range order also increases at those bias voltages. This demonstrates that the fraction of four-coordinated carbon atoms increases and the long-range order of the crystal also increases. On the contrary, for the high bias voltage of $-V_b = 200$ V, the diamond network is damaged: when comparing it to the original structure, the first neighbor peak decreases (indicating that the fraction of four-coordinated carbon atoms decreases), as well as the longer range order, the maximum at 2.95 Å even vanishes. These theoretical results are in full agreement with the experimental results obtained by SEM, Raman spectroscopy and EELS showing that the crystallinity is enhanced at low bias voltages: $-V_b < 140$ V and that the growth of a non-diamond carbon amorphous phase is favored at higher bias voltages ($-V_b > 150$ V).

5 Conclusions Summarized, the crystalline properties of thin diamond layers grown by MW PECVD with different substrate bias voltages have been studied, using several structural, morphological and chemical characterization methods: SEM, TEM, EELS, and Raman spectroscopy. An improvement of the crystalline structure at a bias voltage up to 100–120 V is first observed. Then, at high bias voltages ($-V_b \geq 220$ V), thin films are formed consisting of diamond grains of nanometer size embedded in matrix with a very high concentration of non-diamond phase carbon and a high atomic concentration of hydrogen. Based on the Raman scattering measurements, the Raman line observed at $\sim$1150 cm^{-1} is reassigned to a deformation mode of CH_x bonds in NCD and not to trans-poly-acetylene. This is clearly in disagreement with the current view present inpart of the available literature. In the second part, classical MD simulations have been carried out, supporting the observed experimental data. These theoretical results show an increase of dangling bonds with increasing bias voltage, and point out that the observed exponential rise of the growth rate is not only due to the higher flow of hydrocarbon species, but also to an increase of the carbon incorporation ratio. A close look at the RDF of the simulated cell indicate an improvement of the long range order of the crystal for bias voltages up to 100 V and a further decrease of the crystalline order at higher bias voltages, being in full agreement with the experimental results.

Acknowledgements M.E. and E.N. acknowledge financial support from, respectively, the Institute for Promotion of Innovation through Science and Technology in Flanders (IWT), and the Research Foundation-Flanders (FWO). J.V. gratefully acknowledges financial support from the GOA project "XANES meets ELNES" of the research fund of the University of Antwerp. Calculation support was provided by the University of Antwerp through the core facility CALCUA. G.V.T. acknowledges the ERC grant COUNTATOMS. The work was also financially supported by the joint UA-UHasseltMethusalem "NANO" network, the Research Programs G.0068.07 and G.0555.10N of the Research Foundation-Flanders (FWO), the IAP-P6/42 project "Quantum Effects in Clusters and Nanowires", and by the EU FP7 through the Integrated Infrastructure Initiative "ESMI" (No. 262348), the Marie Curie ITN "MATCON" (PITN-GA-2009-238201), and the Collaborative Project "DINAMO" (No. 245122).

References

[1] A. Krueger, Adv. Mater. **20**, 2444 (2008).
[2] A. Krueger and D. Lang, Adv. Funct. Mater. **22**, 890 (2012).
[3] M. Mkandawire, A. Pohl, T. Gubarevich, V. Lapina, D. Appelhans, G. Rödel, W. Pompe, J. Schreiber, and J. Opitz, J. Biophotonics **2**, 596 (2009).
[4] H. B. Man, R. Lam, M. Chen, E. Osawa, and D. Ho, Phys. Status Solidi A **209**, 1811 (2012), this issue.
[5] G. Balasubramanian, I. Y. Chan, R. Koselov, M. Al-Hmoud, J. Tisler, C. Shin, C. Kim, A. Wojcjk, P. R. Hemmer, A. Krueger, T. Hanke, A. Leitenstorfer, R. Bratschitsch, F. Jelezko, and J. Wrachtrup, Nature **455**, 648 (2008).
[6] O. A. Williams, J. Hees, C. Dieker, W. Jäger, L. Kirste, and C. E. Nebel, ACS Nano **4**, 4824 (2010).
[7] O. A. Williams, O. Douhéret, M. Daenen, K. Haenen, E. Osawa, and M. Takahashi, Chem. Phys. Lett. **445**, 255 (2007).
[8] B. van Grinsven, N. Vanden. Bon, H. Strauven, L. Grieten, M. Murib, S. D. Janssens, K. Haenen, M. J. Schöning, V. Vermeeren, M. Ameloot, L. Michiels, R. Thoelen, W. De Ceuninck, and P. Wagner, ACS Nano **6**, 2712 (2012).
[9] S. Wenmackers, V. Vermeeren, M. vandeVen, M. Ameloot, N. Bijnens, K. Haenen, L. Michiels, and P. Wagner, Phys. Status Solidi A **206**, 391 (2009).
[10] V. Petrakova, A. Taylor, I. Kratochvilova, F. Fendrych, J. Vacik, J. Kucka, J. Stursa, P. Cigler, M. Ledvina, A. Fiserova, P. Kneppo, and M. Nesládek, Adv. Funct. Mater. **22**, 812 (2012).
[11] E. Neu, C. Arend, E. Gross, F. Guldner, C. Hepp, D. Steinmetz, E. Zscherpel, S. Ghodbane, H. Sternschulte, D. Steinmuller-Nethl, Y. Liang, A. Krueger, and C. Becher, Appl. Phys. Lett. **98**, 243107 (2011).
[12] Y.-G. Lu, S. Turner, J. Verbeeck, S. D. Janssens, P. Wagner, K. Haenen, and G. Van Tendeloo, Appl. Phys. Lett **101**, 041907 (2012).
[13] S. Turner, Y.-G. Lu, S. D. Janssens, F. Da Pieve, D. Lamoen, J. Verbeeck, K. Haenen, P. Wagner, and G. Van Tendeloo, Nanoscale (2012), DOI: 10.1039/C2NR31530K.
[14] N. Jiang, K. Sugimoto, K. Eguchi, T. Inaoka, Y. Shintani, H. Makita, A. Hatta, and A. Hiraki, J. Cryst. Growth **222**, 591 (2001).
[15] M. Schreck, T. Baur, R. Fehling, M. Muller, B. Stritzker, A. Bergmaier, and G. Dollinger, Diam. Relat. Mater. **7**, 293 (1998).
[16] C. Z. Guand and X. Jiang, J. Appl. Phys. **88**, 1788 (2000).
[17] V. Mortet, M. Daenen, T. Teraji, A. Lazea, V. Vorlicek, J. D'Haen, K. Haenen, and M. D'Olieslaeger, Diam. Relat. Mater. **17**, 1330 (2008).
[18] S. Katai, Z. Tass, G. Hars, and P. Deak, J. Appl. Phys. **86**, 5549 (1999).
[19] W. Kulish, L. Ackermann, and B. Sobisch, Phys. Status Solidi A **154**, 155 (1996).
[20] J. S. Lee, K. S. Liu, and L.-N. Lin, Appl. Phys. Lett. **67**, 1555 (1995).
[21] K. Byrappa and T. Ohachi, Crystal Growth Technology (William Andrew & Springer, New York, 2003), p. 111.
[22] I.-H. Choi, P. Weisbecker, S. Barrat, and E. Bauer-Grosse, Diam. Relat. Mater. **13**, 574 (2004).
[23] O. A. Williams, M. Nesládek, M. Daenen, S. Michaelson, A. Hoffman, E. Ōsawa, K. Haenen, and R. B. Jackman, Diam. Relat. Mater. **17**, 1080 (2008).
[24] R. W. Bormett, S. A. Asher, R. E. Witowski, W. D. Partlow, R. Lizewski, and F. Pettit, J. Appl. Phys. **77**, 5916 (1995).
[25] A. C. Ferrari and J. Robertson, Phys. Rev. B **63**, 121405(R). (2001).
[26] H. Kuzmany, R. Pfeiffer, N. Salk, and B. Gunther, Carbon **42**, 911 (2004).
[27] T. Lopez-Rios, E. Sandre, S. Leclercq, and E. Sauvain, Phys. Rev. Lett. **76**, 4935 (1996).
[28] H. Boppart, J. van Straaten, and I. Silver, Phys. Rev. B **32**, 1423 (1985).
[29] M. Yoshikawa, Y. Yuri, M. Maegawa, G. Katagiri, H. Ishida, and A. Ishitani, Appl. Phys. Lett. **62**, 3114 (1993).

[30] R. J. Nemanich, S. A. Solin, and R. M. Martin, Phys. Rev. B **23**, 6348 (1981).
[31] J.-Y. Kim, E.-R. Kim, D.-W. Ihm, and M. Tasumi, Bull. Korean Chem. Soc. **23**, 1404 (2002).
[32] S. H. Michaelson and A. Hoffman, Diam. Relat. Mater. **15**, 486 (2006).
[33] C. Wild, N. Herres, and P. Koild, J. Appl. Phys. **68**, 973 (1990).
[34] G. Bertoni, E. Beyers, J. Verbeeck, M. Mertens, P. Cool, E. F. Vansant, and G. Van Tendeloo, Ultramicroscopy **106**, 630 (2006).
[35] J. Verbeeck and S. Van Aert, Ultramicroscopy **101**, 207 (2004).
[36] O. A. Williams, M. Daenen, J. D'Haen, K. Haenen, M. Nesládek, and D. M. Gruen, Diam. Relat. Mater. **15**, 654 (2006).
[37] M. Eckert, E. Neyts, and A. Bogaerts, Chem. Vap. Deposition **14**, 213 (2008).
[38] A. Hoffman, I. Gouzman, and S. H. Michaelson, Thin Solid Films **515**, 14 (2006).
[39] J. Robertson, J. Gerber, S. Sattel, M. Weiler, K. Jung, and H. Ehrhardt, Appl. Phys. Lett. **66**, 3287 (1995).
[40] D. Frenkel and B. Smit, Understanding Molecular Simulation (Academic Press, San Diego, 1996).
[41] J. Tanaka, C. F. Abrams, and D. B. Graves, J. Vac. Sci. Technol. A **18**, 938 (2000).
[42] D. W. Brenner, Phys. Rev. B **42**, 9458 (1990).
[43] S. H. Michaelson, R. Akhvlediani, A. Hoffmann, A. Silverman, and J. Adler, Phys. Status Solidi A **205**, (2099). (2008).
[44] H. J. C. Berendsen, J. P. M. Postma, W. F. van Gunsteren, A. DiNola, and J. R. Haak, J. Chem. Phys. **81**, 3684 (1984).
[45] H. D. Hagstrum, Phys. Rev. **122**, 83 (1961).
[46] P. W. May, J. N. Harvey, J. A. Smith, and Yu. A. Mankelevich, J. Appl. Phys. **99**, 104907 (2006).

